

Super-horizon primordial black holes

^{1,2}Tomohiro Harada* and ¹B. J. Carr†

¹*Astronomy Unit, School of Mathematical Sciences, Queen Mary,
University of London, Mile End Road, London E1 4NS, UK*

²*Department of Physics, Kyoto University, Kyoto 606-8502, Japan*

(Dated: July 8, 2018)

We discuss a new class of solutions to the Einstein equations which describe a primordial black hole (PBH) in a flat Friedmann background. Such solutions arise if a Schwarzschild black hole is patched onto a Friedmann background via a transition region. They are possible providing the black hole event horizon is larger than the cosmological apparent horizon. Such solutions have a number of strange features. In particular, one has to define the black hole and cosmological horizons carefully and one then finds that the mass contained within the black hole event horizon decreases when it is larger than the Friedmann cosmological apparent horizon, although its area always increases. These solutions involve two distinct future null infinities and are interpreted as the conversion of a white hole into a black hole. Although such solutions may not form from gravitational collapse in the same way as standard PBHs, there is nothing unphysical about them, since all energy and causality conditions are satisfied. Their conformal diagram is a natural amalgamation of the Kruskal diagram for the extended Schwarzschild solution and the conformal diagram for a black hole in a flat Friedmann background. In this paper, such solutions are obtained numerically for a spherically symmetric universe containing a massless scalar field, but it is likely that they exist for more general matter fields and less symmetric systems.

PACS numbers: 04.70.Bw, 97.60.Lf, 04.25.Dm, 95.35.+d

I. INTRODUCTION

In a recent paper [1] (henceforth Paper I) we studied numerically the growth of primordial black holes (PBHs) in a universe containing a massless scalar field but no other matter. Following Hamadé and Stewart [2], the double-null formulation of the Einstein equations was used. This is a powerful tool for investigating regions outside the cosmological horizon and inside the black hole horizon simultaneously. On the assumption that the PBH is formed from a local initial density perturbation which propagates causally, the black hole was modelled by matching a Schwarzschild solution to an exact flat Friedmann solution across a null surface. Initial data were specified on an outgoing and ingoing null surface. They were assumed to be exactly Friedmann on the outgoing surface and outside the matching boundary on the ingoing surface but some perturbation of Friedmann inside the matching boundary.

In all the solutions considered in Paper I, the black hole event horizon (BHEH) was assumed to be smaller than the cosmological apparent horizon. However, in some circumstances (e.g. in the inflationary scenario), the perturbation - and perhaps even the black hole itself - may extend well beyond it. In this case, the only upper limit on its size comes from requiring that the perturbed region be part of our universe rather than a separate closed universe. The condition for this has been derived precisely for the situation in which the collapsing region is homogeneous and the equation of state is $p = k\rho$ [3]. In particular, this includes the massless scalar field case, since this is equivalent to a stiff fluid with $k = 1$ providing the gradient of the field is everywhere timelike and vorticity free (as expected). The peculiarity of the formation of PBHs in a universe with a stiff fluid was discussed in Ref. [4], and this suggests that the gradient of the scalar field could have an important hydrodynamical effect.

We study such “super-horizon” solutions in this paper, although our numerical results only cover the scalar field case. It turns out that these scalar field solutions have some rather strange properties. For example, the mass contained within the BHEH decreases when the PBH is larger than the cosmological apparent horizon, although the area always increases. Since our system satisfies all energy conditions, the mass decrease of super-horizon PBHs we show here is completely different from the black hole mass decrease due to phantom energy accretion [5]. Also the conformal diagram for these solutions is interesting, being a natural extension of the Kruskal diagram to the cosmological context. The scalar field usually has a timelike gradient in the numerical simulations shown here and this means that it is equivalent to a stiff fluid. It is likely that there are analogues of these solutions for more general fluids with $p = k\rho$ providing $k > 1/3$. However, we do not study these solutions here. In all these cases, we need to

* Electronic address: harada@scphys.kyoto-u.ac.jp

† Electronic address: B.J.Carr@qmul.ac.uk

define cosmological and black hole horizons very carefully when their sizes are all of the same order.

II. FORMULATION

A. Double-Null Formulation of Einstein equations

As in paper I, we consider a massless scalar field Ψ in general relativity, for which the stress-energy tensor is

$$T_{ab} = \Psi_{,a}\Psi_{,b} - \frac{1}{2}g_{ab}\Psi^{,c}\Psi_{,c}. \quad (2.1)$$

The Einstein equations are

$$R_{ab} - \frac{1}{2}g_{ab}R = 8\pi T_{ab}, \quad (2.2)$$

and the equation of motion for the scalar field is

$$\square\Psi = \Psi^{;a}{}_{;a} = 0. \quad (2.3)$$

We focus on a spherically symmetric system, for which the line element can be written in the form

$$ds^2 = -a^2(u, v)dudv + r^2(u, v)(d\theta^2 + \sin^2\theta d\phi^2), \quad (2.4)$$

where u and v are advanced and retarded time coordinates, respectively, a is the metric function and r is the ‘‘area radius’’ (the proper area of the sphere of constant r being $4\pi r^2$). Equations (2.2) and (2.3) then imply that we have 14 first-order partial differential equations and two auxiliary equations. These equations are given explicitly in Section 2 of [2]. We adopt units in which $G = c = 1$.

B. Misner-Sharp mass and trapping horizons

The existence and position of marginal surfaces can be inferred from the form of the Misner-Sharp mass [6]. This is a well-behaved quasi-local mass in spherically symmetric spacetimes [7], which can be written as

$$m = \frac{r}{2} \left(1 + \frac{4r_{,u}r_{,v}}{a^2} \right). \quad (2.5)$$

Combining this with the equations in Section 2 of [2], we can derive the following useful relations:

$$m_{,u} = -\frac{8\pi r^2 r_{,v} (\Psi_{,u})^2}{a^2}, \quad (2.6)$$

$$m_{,v} = -\frac{8\pi r^2 r_{,u} (\Psi_{,v})^2}{a^2}. \quad (2.7)$$

In this paper, we adopt the ‘‘trapping horizon’’ framework introduced by Hayward [7, 8] because this provides a systematic and mathematically transparent view of the sort of cosmological black holes treated here. In the context of this paper, trapping horizons and conventional apparent horizons are almost equivalent but they need not be in more general situations.

Although the values for $r_{,v}$ and $r_{,u}$ are not geometrical invariants, their signs are, which leads to the following definitions. (i) A metric sphere is said to be trapped if $r_{,v}r_{,u} > 0$. A sphere with $r_{,u} < 0$ and $r_{,v} < 0$ is future trapped, while one with $r_{,u} > 0$ and $r_{,v} > 0$ is past trapped. (ii) A metric sphere is said to be untrapped if $r_{,v}r_{,u} < 0$. On an untrapped surface, ∂_v is outgoing if $r_{,v} > 0$ and ingoing if $r_{,v} < 0$. More generally, a spacelike or null normal vector z^a is outgoing if $z^a r_{,a} > 0$ and ingoing if $z^a r_{,a} < 0$. (iii) A metric sphere is said to be marginal if $r_{,v}r_{,u} = 0$. A sphere with $r_{,v} = 0$ is future marginal if $r_{,u} < 0$, past marginal if $r_{,u} > 0$ and bifurcating marginal if $r_{,u} = 0$. It is described as outer marginal if $r_{,uv} < 0$, inner marginal if $r_{,uv} > 0$ and degenerate marginal if $r_{,uv} = 0$. It is easily seen that a sphere is marginal if and only if $r = 2m$, trapped if and only if $r < 2m$ and untrapped if and only if $r > 2m$.

The closure of a hypersurface foliated by a future or past, outer or inner marginal sphere is called a (nondegenerate) trapping horizon. In Hayward’s approach, the black hole apparent horizon is replaced with a ‘‘future outer trapping

horizon” (FOTH), while the cosmological (white hole) apparent horizon is replaced with a “past outer trapping horizon” (POTH). There is a critical difference between an apparent horizon and a trapping horizon. An apparent horizon is defined only on a prescribed spacelike hypersurface, which is usually required to be a Cauchy surface, so it exists only if the spacetime is strongly asymptotically predictable [9]. On the other hand, a trapping horizon is the trajectory of a marginal surface in the whole spacetime, and it is defined locally whenever a null foliation is possible. The spacetime does not need to be strongly asymptotically predictable. It should be stressed that Hawking’s “area theorem” [10] only refers to the BHEH. On the other hand, Hayward has shown that it also applies for a FOTH providing the null energy condition holds.

Providing the black hole horizon is within the cosmological horizon and u and v are the standard double-null coordinates in the asymptotic Friedmann region, the FOTH and the POTH correspond to the conditions $r_{,v} = 0$ and $r_{,u} = 0$, respectively. However, the situation is more complicated if the black hole horizon is outside the cosmological horizon. In this case, we can still define trapping horizons by the conditions $r_{,v} = 0$ and $r_{,u} = 0$, but these are no longer everywhere identified with a FOTH and a POTH. Using the above equations, we can show that along a trapping horizon, on which $r = 2m$, we have

$$[a^2 r_{,u} + 16\pi r^2 r_{,v} (\Psi_{,u})^2] du + [a^2 r_{,v} + 16\pi r^2 r_{,u} (\Psi_{,v})^2] dv = 0. \quad (2.8)$$

On trapping horizons, which have $r_{,v} = 0$ and $r_{,u} = 0$, we therefore have

$$a^2 du + 16\pi r^2 (\Psi_{,v})^2 dv = 0, \quad (2.9)$$

$$16\pi r^2 (\Psi_{,u})^2 du + a^2 dv = 0, \quad (2.10)$$

respectively. We conclude that trapping horizons are non-timelike in this system. More precisely, a trapping horizon with $r_{,v} = 0$ has $u = \text{const}$ if and only if $\Psi_{,v} = 0$, while a trapping horizon with $r_{,u} = 0$ has $v = \text{const}$ if and only if $\Psi_{,u} = 0$. Except for these special cases, trapping horizons are spacelike.

The form of $a(u, v)$ and $r(u, v)$ in the exact flat Friedmann model is given in Appendix B of Paper I. This implies that the cosmological particle horizon has $u = 0$, while the cosmological apparent horizon, which is a POTH, has $3u + v = 0$. This shows that the cosmological apparent horizon is spacelike and outside the particle horizon. The conformal diagram of the spacetime is indicated in Fig. 1, which shows the initial (big bang) spacelike singularity. The cosmological apparent horizon also coincides with the Hubble horizon in this case. If one has a black hole embedded in an exact or asymptotically flat Friedmann model and smaller than the cosmological particle horizon, the conformal diagram will change to the form indicated in Fig. 2. This now contains a BHEH, a FOTH and a final (black hole) spacelike singularity.

III. INITIAL DATA FOR PBHS

A. Structure of initial data

The initial data are prescribed on the two null surfaces $u = u_0$ and $v = v_0$, with the region of calculation being the diamond $[u_0, u_1] \times [v_0, v_1]$. We have three independent functions on the two null surfaces: a , Ψ and r . Two of them can be chosen freely and the third is determined by the constraint equations on the null surfaces. It is convenient to choose

$$a(u_0, v), a(u, v_0), \Psi(u_0, v), \Psi(u, v_0) \quad (3.1)$$

as the free initial data and to regard

$$r(u_0, v), r(u, v_0) \quad (3.2)$$

as being determined by the initial value equations. We can regard $\Psi(u_0, v)$ and $\Psi(u, v_0)$ as the physical degrees of freedom in the initial data, while the choice for $a(u_0, v)$ and $a(u, v_0)$ fixes the gauge.

In the flat Friedmann region, we adopt the coordinate system given in Appendix B1 of Paper I and impose flat Friedmann initial data for a and Ψ on $u = u_0$ for $v_0 \leq v \leq v_1$. On $v = v_0$, we also choose flat Friedmann data for a for $u_0 \leq u \leq u_1$. For Ψ , we use the same data on the initial null surface $v = v_0$ for $u_0 \leq u \leq u_m$, but $\Psi = \text{const}$ for $u_m + \Delta u < u \leq u_1$. This is equivalent to Schwarzschild data in coordinates penetrating the black hole. The sudden transition from flat Friedmann data to Schwarzschild data results in a discontinuity at $u = u_m$, which reduces the numerical accuracy. Hence we smooth the transition with some smoothing length Δu ; we use a quadratic function

between u_m and $u_m + \Delta u$, so that Ψ and $\Psi_{,u}$ are continuous. More precisely, we impose the following initial data for a and $s \equiv \sqrt{4\pi\Psi}$:

$$a^2(u, v_0) = C^2 \left(\frac{u + v_0}{2} \right), \quad (3.3)$$

$$s(u, v_0) = \begin{cases} \frac{\sqrt{3}}{2} \ln \left(\frac{u + v_0}{2} \right) + s_0 & (u < u_m) \\ \frac{\sqrt{3}}{2} \left[\frac{(\Delta u)^2 - (u_m + \Delta u - u)^2}{2\Delta u(u_m + \Delta u)} + \ln \left(\frac{u_m + v_0}{2} \right) \right] + s_0 & (u_m \leq u < u_m + \Delta u) \\ \frac{\sqrt{3}}{2} \left[\frac{\Delta u}{2(u_m + v_0)} + \ln \left(\frac{u_m + v_0}{2} \right) \right] + s_0 & (u \geq u_m + \Delta u) \end{cases}, \quad (3.4)$$

on the initial null surface $v = v_0$, and

$$a^2(u_0, v) = C^2 \left(\frac{u_0 + v}{2} \right), \quad (3.5)$$

$$s(u_0, v) = \frac{\sqrt{3}}{2} \ln \left(\frac{u_0 + v}{2} \right) + s_0, \quad (3.6)$$

on the initial null surface $u = u_0$. Here C and s_0 are constants and, without loss of generality, we can choose $C = 1$ and $s_0 = 0$. Note that although one has a Schwarzschild vacuum for $u \geq u_m + \Delta u$, this situation only applies instantaneously at $v = v_0$, since the inflowing matter will fill this up immediately.

Figure 3 depicts the initial data for our numerical simulations, these being completely determined by the two parameters u_m and Δu . When the matching region is very narrow, the BHEH is smaller than the Friedmann cosmological apparent horizon if $u_m > u_{\text{CAH}}(v_0)$. This corresponds to Fig. 3(a), where $u = u_{\text{CAH}}(v)$ denotes the trajectory of the cosmological apparent horizon. However, if $u_m < u_{\text{CAH}}(v_0)$, the BHEH is larger than the Friedmann cosmological horizon, which corresponds to Fig. 3(b). Note that the cosmological apparent horizon would always go within the matching radius if one took v_0 small enough, so when the black hole forms is crucial. Note also that when we refer to a POTH in the background Friedmann model, we refer to it as the (Friedmann) cosmological apparent horizon. As discussed later, this relates to the distinction between a black hole that forms from collapse and an eternal black hole that exists “ab initio”.

IV. RESULTS

A. Black hole event horizon

Our numerical code is based on that of Hamadé and Stewart [2] with a modification, described in Appendix A of Paper I, to ensure greater accuracy. The initial data are prescribed on the two null surfaces $v = v_0 = 1$ and $u = u_0 = -2/3$, this also fixing the units. The calculated region is the diamond contained by $u = u_0$, $v = v_0$, $u = u_1$ and $v = v_1$. On the initial null surface $v = v_0$, we make the matching at $u = u_m$ and use the smoothing length Δu . As time proceeds, the $u = \text{const}$ null rays will become ever more sensitive to r near the BHEH, so the calculation is stopped at $v = v_1$, when the null rays become too coarse to be resolved. The parameters used are summarised in Table I for six models. The BHEH is identified as the critical null ray $u = u_{\text{BHEH}}$, the null rays with $u < u_{\text{BHEH}}$ going to $r = \infty$ and those with $u > u_{\text{BHEH}}$ returning to $r = 0$. Therefore, the BHEH is only identified at the end of the calculation. Although the identification of the BHEH is rather imprecise, because of numerical errors and the finiteness of the calculated regions, it suffices for the physical interpretation of the results given below. It is found that all six models have a BHEH and Table I indicates the initial ratio of the sizes of the BHEH and the Friedmann cosmological apparent horizon at $v = v_0$. This complements Table I of Paper I, which only shows cases (A to D) in which the ratio is less than 1. All models except E have an initial BHEH larger than the Friedmann cosmological apparent horizon. In Model E the initial BHEH is slightly smaller than the Friedmann cosmological apparent horizon.

B. Location of horizons

Figure 4 shows the locations of the BHEH and trapping horizons in the (u, v) plane. It also indicates the signs of $r_{,v}$ and $r_{,u}$. The region is future trapped if the signs are $(-, -)$, past trapped if they are $(+, +)$ and untrapped if they are $(+, -)$ or $(-, +)$. Trapping horizons may have either $r_{,v} = 0$ or $r_{,u} = 0$.

TABLE I: Model parameters and the initial mass ratios of BHEH to the Friedmann cosmological apparent horizon.

Models	u_m	Δu	u_0	u_1	v_0	v_1	$m_{\text{BHEH}}/m_{\text{CAH}}$
E	-1/2	0.4	-2/3	2	1	4.5	0.969
F	-1/2	0.02	-2/3	2	1	4.5	2.12
G	-1/2	0.05	-2/3	2	1	4.5	2.01
H	-1/2	0.2	-2/3	2	1	4.5	1.52
I	-0.6	0.02	-2/3	2	1	4.5	3.58
J	-0.4	0.02	-2/3	2	1	4.5	1.31

There are two qualitatively different classes of models. In the first class, which includes all models except E, the initial BHEH is larger than the Friedmann cosmological apparent horizon. As seen from the figure, as v increases from $v_0 = 1$, two trapping horizons, one with $r_{,v} = 0$ and the other with $r_{,u} = 0$, appear and cross each other in the future of the BHEH. In terms of the evolution with respect to v , before the crossing the trapping horizons with $r_{,v} = 0$ and $r_{,u} = 0$ correspond to a POTH and a FOTH, respectively. After the crossing, the situation is reversed, so the trapping horizons with $r_{,v} = 0$ and $r_{,u} = 0$ correspond to a FOTH and a POTH, respectively. After further evolution, the POTH crosses the BHEH. Thereafter it will coincide with the Friedmann cosmological apparent horizon, while the FOTH corresponds to the black hole apparent horizon.

In the second class of models, which includes E, the initial BHEH is smaller than the Friedmann cosmological apparent horizon. Trapping horizons with $r_{,v} = 0$ and $r_{,u} = 0$ appear and remain in the future and past of the BHEH, respectively. These two trapping horizons do not cross each other and always correspond to the FOTH and POTH, respectively.

C. PBH mass change

The area radii of the BHEH and trapping horizons for these models are shown in Fig. 5. It is seen that the area of the BHEH always increases for these models, which is consistent with the black hole area theorem [10]. If the initial BHEH is larger than the Friedmann cosmological apparent horizon, i.e., for all models other than E, the areas of the trapping horizons with both $r_{,v} = 0$ and $r_{,u} = 0$ first decrease as v increases and then increase after crossing each other. It is interesting that, in terms of v , the two trapping horizons cross at a radius slightly larger than the BHEH at the crossing time. After the BHEH enters the future of the POTH, it soon gets much smaller than it. For these models, the FOTH appears just before the trapping horizons cross, although this is not so clear in the figure. For models where the initial BHEH is smaller than the Friedmann cosmological apparent horizon, i.e., Model E, the situation is standard. In terms of r , the FOTH is inside the BHEH, while the POTH is outside it. The BHEH soon gets much smaller than the POTH.

Figure 6 shows the evolution of the Misner-Sharp mass of the BHEH and trapping horizons. For models where the initial BHEH is larger than the Friedmann cosmological apparent horizon, the mass of the BHEH first decreases and then increases. As we will see later, the mass of the BHEH decreases if and only if it is in the past trapped region. When the black hole gets out of the past trapped region, its mass starts to increase. The mass of the trapping horizon with $r_{,v} = 0$ is only slightly smaller than that of the BHEH, despite the radii being considerably different. This is because the density inside the perturbed region is very small. After the BHEH crosses the trapping horizon with $r_{,u} = 0$, which is a POTH at the crossing, the mass of the BHEH soon gets much smaller than the mass of the cosmological apparent horizon.

The change in the BHEH mass may be seen more clearly in Fig. 7, which shows the rate of mass increase dm_{BHEH}/dv . For models other than E, this is initially negative but it then increases, crosses zero, reaches a positive maximum and then decreases. The larger the initial mass ratio of the BHEH to the Friedmann cosmological apparent horizon, the more negative the initial mass increase rate is. For Model E, where the initial BHEH is slightly smaller than the Friedmann cosmological apparent horizon, the accretion rate starts with a very small positive value, increases to a maximum and then decreases. The behaviour of the BHEH mass is clearly explained by Eq. (2.7), which can be rewritten as a black hole mass equation:

$$\frac{dm_{\text{BHEH}}}{dt} = -8\pi r^2 \frac{(\Psi_{,v})^2}{a^2} \left(\frac{dr}{dt} \right)_{v=\text{const}}, \quad (4.1)$$

where $t = t(u+v)$ is any time coordinate which depends on $u+v$. Whether the black hole mass increases or decreases depends solely on the sign of $r_{,u}$, which is the null expansion along the $v = \text{const}$ direction. In the usual situation,

the BHEH is in a region where $r_{,u} < 0$ and its mass monotonically increases. However, when the BHEH is in a past trapped region, its mass monotonically decreases because $r_{,u} > 0$. Equation (4.1) (or (2.7)) also explains why the mass accretion rate starts very small for Model E. Since the BHEH is inside but very close to the cosmological apparent horizon, $r_{,u}$ starts off negative but very close to zero. After some evolution, $r_{,u}$ decreases well below zero and the accretion then increases. This suppression of accretion for a PBH as large as a cosmological apparent horizon is due purely to general relativistic effects, or relativistic cosmological expansion. Paper I discusses the qualitative difference between PBHs whose size is comparable to and much smaller than the cosmological apparent horizon.

For models with the initial BHEH larger than the Friedmann cosmological apparent horizon, the areas and masses of both trapping horizons decrease as v increases before they cross each other. After the crossing, they increase. This behaviour is completely consistent with the “second law” for trapping horizons, as formulated by Hayward [7]. The theorem states, for example, that if the null energy condition holds, then the area and mass of the FOTH (POTH) with $r_{,v} = 0$ do not decrease (increase) along the vector z tangent to the horizon. This vector has the form $z = \beta\partial_v - \alpha\partial_u$ where $\beta > 0$.

D. Conversion from a white hole to a black hole

To understand the spacetime structure for solutions in which the PBH is larger than the cosmological apparent horizon, we concentrate on Model F. Figure 8 gives the detailed numerical results for this model. Figures 8(a) and (b) give the evolution of r along the null geodesics with $v = \text{const}$ and $u = \text{const}$, respectively, while Figs. 8 (c) and (d) give that of $2m/r$ along the null geodesics with $v = \text{const}$ and $u = \text{const}$, respectively. It is seen that r continues to increase along both the earlier null geodesics with $u = \text{const}$ and $v = \text{const}$. This is also consistent with Fig. 4 (a). On the initial null ray $v = v_0 = 1$, $2m/r$ decreases monotonically as u increases and crosses unity from above, as can be seen in Fig. 4(c). Since we have chosen $\Psi = \text{const}$ for $u \geq u_m + \Delta u$ on the initial null ray $v = v_0$, Eq. (2.6) implies $m = \text{const}$ here. Since $r_{,u} = 0$ implies $2m/r = 1$, the area radius along the null ray $v = v_0$ must monotonically increase as u increases. This means that this null ray does not reach $r = 0$ but another null infinity, different from the one which the null rays with $u = \text{const}$ reach.

We can now see that the standard conformal diagram for PBHs, which is given by Fig. 2, will not apply if the BHEH is larger than the cosmological apparent horizon. Rather the conformal diagram is given by Fig. 9. The FOTH and POTH intersect at one point in this diagram. This point corresponds to a sphere which is a bifurcating marginal surface. It is clear that the spacetime can be interpreted as the conversion of a white hole to a black hole, since a PBH larger than the cosmological apparent horizon involves a past trapped region changing to a future trapped one. There are two distinct asymptotic regions: the future null infinity for rays with $u = \text{const}$ and the one for rays with $v = \text{const}$. These two asymptotic regions are associated with two disconnected untrapped regions. It is impossible for an observer to go from one untrapped region to the other by traversing the crossing point, the future trapped or past trapped region. The spacetime has no regular centre.

Figure 9 is naturally interpreted as an amalgamation of the Kruskal diagram for the extended Schwarzschild solution, shown in Fig. 10, and the standard conformal diagram for a black hole in a flat Friedmann background, shown in Fig. 2. It will be recalled that the Kruskal diagram also contains a white hole changing into a black hole and two asymptotically flat regions. The analogy of this extension for the conformal diagram shown in Fig. 2 is shown in Fig. 11. This contains the big bang singularity, the black hole singularity and two asymptotically flat Friedmann regions. There are two BHEHs and two POTHs, these crossing in the black hole region. The regions below the two POTHs are past trapped but not precisely equivalent to a white hole since, unlike the situation in Fig. 10, there are no past null infinities and no past event horizons. Since the spacetime has no regular centre, it cannot contain a particle horizon as a light cone which emanates from the regular centre just after the big bang. Figure 9 is obviously contained within Fig. 11 but the present numerical calculations do not determine what happens in the region $v < v_0$.

V. DISCUSSION

If we accept both the conventional conformal diagram for PBHs shown in Fig. 2 and the new one shown in Fig. 9 or Fig. 11, we have two distinct PBH causal structures. The conventional diagram has a regular centre $r = 0$ and a single null infinity, while the new one has no regular centre and two null infinities. This raises the issue of what determines the causal structure of PBH spacetimes. If we consider standard PBH formation from initial data with a regular centre, then the causal structure will be described by the conventional diagram.

Another issue concerns the transition between the two diagrams. If this transition is governed by parameters which can be changed continuously, it would be natural to assume that there is a threshold spacetime which separates them. We should note that the BHEH is null, while the cosmological apparent horizon is spacelike in the massless scalar

field case (see Fig. 3). Hence, if the u_{BHEH} is smaller than $u = u_{\text{CPH}}$ of the cosmological particle horizon (0 in the present coordinates), the BHEH can be always outside the cosmological apparent horizon if we take v_0 sufficiently small. In this case, $m_{\text{BHEH}}(v_0) > m_{\text{CAH}}(v_0)$ and hence the causal structure should be given by Fig. 9 or Fig. 11. On the other hand, if $u_{\text{BHEH}} > u_{\text{CPH}}$, the causal structure is depicted by Fig. 2 and the spacetime has a regular centre before the BHEH appears. Therefore, the transition spacetime corresponds to a PBH whose event horizon coincides with the cosmological particle horizon of the background cosmological solution. The causal structure of this critical spacetime is depicted in Fig. 12.

The discussion of the mass variation of the BHEH can be understood in the more general spherically symmetric context from the counterparts of Eqs. (2.6) and (2.7) [3, 7]. In our notation, these equations become

$$m_{,u} = \frac{8\pi r^2}{a^2}(T_{uv}r_{,u} - T_{uu}r_{,v}), \quad (5.1)$$

$$m_{,v} = \frac{8\pi r^2}{a^2}(T_{uv}r_{,v} - T_{vv}r_{,u}). \quad (5.2)$$

The combination of the two terms in parentheses on the right-hand side of Eq. (5.2), related to null expansions, determines the time variation of the BHEH mass. In the case of a massless scalar field, the situation is simplified because $T_{uv} = 0$ and $T_{vv} = (\Psi_{,v})^2 \geq 0$. We therefore conclude that the black hole accretion vanishes when the event horizon coincides with the POTH with $r_{,u} = 0$ and that it becomes negative when the event horizon is in a past trapped region. For general matter fields, it can be proved that the BHEH mass is non-decreasing if $r_{,v} > 0$, $r_{,u} < 0$ and the dominant energy condition hold on the event horizon (c.f. Proposition 5 of [7]). However, if these assumptions are not satisfied, the mass variation of the BHEH is non-trivial. If the dominant energy condition holds, then the conditions $T_{uv} \geq 0$ and $T_{vv} \geq 0$ are necessarily satisfied. In the general case with $T_{uv} > 0$, the BHEH mass still increases even when it is on a POTH with $r_{,u} = 0$. When the BHEH is in a past trapped region, the first and second terms in parentheses on the right-hand side of Eq. (5.2) make positive and negative contributions, respectively, to the black hole mass change. Even when the BHEH is in a past trapped region, its mass can still increase if the first term is dominant. This suggests that the BHEH has to be well outside the POTH in order to have suppressed accretion or mass decrease for general matter fields satisfying the dominant energy conditions. On the other hand, there could still be a lot of accretion for some other kinds of matter field.

We have shown that the mass of the BHEH can decrease even if all possible energy and causality conditions hold. This suggests that the usual concept of event horizons is not appropriate for a proper discussion of black hole thermodynamics. This is why Hayward [7, 8, 11, 12] introduced the concept of the FOTH (POTH) as a useful generalisation of the idea of a black hole (white hole) event horizon. As we saw in Section II B, the idea is that all definitions should be quasi-local and this is useful in proving black hole properties. For example, when the black hole (white hole) horizon is defined as a FOTH (POTH), one can prove the monotonicity of the area and mass in the spherically symmetric situation. From this point of view, Fig. 9 describes the conversion of a white hole to a black hole by definition.

Although the analysis in this paper has assumed spherical symmetry, it is likely that similar considerations apply more generally. If we consider slightly nonspherical PBH spacetimes, it is trivial to show that the strange properties discussed in this paper still hold. However, when the system is very far from spherical symmetry, we need to re-analyse the Einstein equations. Although the conditions for suppressed accretion or mass reduction may change, we believe the appearance of these properties is robust.

Since a spacetime which contains a PBH larger than the cosmological apparent horizon cannot have a regular centre, such PBHs could not form through classical processes from a Friedmann background. This implies that a PBH formed through classical processes always increases its mass and soon gets much smaller than the cosmological horizon even if it is comparable with the cosmological scale at its formation. On the other hand, if we take quantum processes or inflation preceding to the massless scalar field dominated stage into account, the formation of such PBHs may be allowed. Moreover, there is a possibility that the universe initially contained a past trapped region which was converted into a future trapped region, as indicated in Fig. 11. This kind of PBH might be described as “ab initio” or “eternal”.

VI. CONCLUSION

We have investigated PBHs in a flat Friedmann universe with a massless scalar field which are larger than the cosmological apparent horizon. Through fully general relativistic numerical calculations, we have found that there are two trapping horizons which cross. This corresponds to the conversion of a white hole into a black hole and to an initial reduction in the mass of the black hole event horizon. We have seen that these unusual features are peculiar to PBHs larger than the cosmological apparent horizon.

The present analysis is confined to the spherically symmetric situation with a massless scalar field, so it is clearly important to examine how sensitive these peculiar features are to the assumed symmetry and type of matter field. In particular, it is interesting to study whether the condition for the black hole mass reduction applies more generally. If so, this will be important for black hole physics and black hole thermodynamics. It is also interesting to study under what circumstances such a PBH can arise in the early universe, especially in the context of inflationary cosmology, and how this relates to the separate universe condition. To make such an extension numerically or analytically, it would be very important to adopt the appropriate definition of the cosmological and black hole horizons and the trapping horizon framework should be suitable for the case in which the black hole is as large as the cosmological horizon. We will study these issues in a future paper.

The formation of PBHs arising from the evolution of an effectively massless scalar field during inflation and its implication for the formation of galaxies and supermassive black holes in galactic nuclei has been recently discussed in Ref. [13]. In this scenario, super-horizon PBHs may naturally arise due to the closed domain walls of size exceeding the cosmological horizon.

Finally, it should be noted that the conversion of a wormhole to a black hole in a first order phase transition was studied in Ref. [14] in the context of bubble nucleation. They showed that if a wormhole is created in the transition from a false to a true vacuum, it necessarily collapses to a black hole. Since our system only contains a scalar field with no potential and therefore no phase transition, the situation is rather different. However, it is quite interesting that similar phenomena are seen in different systems.

Acknowledgments

We would thank S. A. Hayward for helpful comments and clarifying trapping horizon notation. TH is grateful to K. Nakao for helpful comments. TH was partly supported from JSPS. This work was partly supported by the Grant-in-Aid for the 21st Century COE “Center for Diversity and Universality in Physics” from the Ministry of Education, Culture, Sports, Science and Technology (MEXT) of Japan.

-
- [1] T. Harada and B. J. Carr, *Phys. Rev. D* **71**, 104010 (2005).
 - [2] R. S. Hamadé and J. M. Stewart, *Class. Quantum Grav.* **13**, 497 (1996).
 - [3] T. Harada and B. J. Carr, *Phys. Rev. D* **71**, 104009 (2005).
 - [4] N. A. Zaboltn and P. D. Nasel’skii, *Sov. Astron. Lett.* **6**, 7 (1980).
 - [5] E. Babichev, V. Dokuchaev and Yu. Eroshenko, *Phys. Rev. Lett.* **93**, 021102 (2004); *J. Ex. Th. Phys.* **100**, 528 (2005).
 - [6] C. W. Misner and D. H. Sharp, *Phys. Rev.* **136**, B571 (1964).
 - [7] S. A. Hayward, *Phys. Rev. D* **53**, 1938 (1996).
 - [8] S. A. Hayward, *gr-qc/9303006*.
 - [9] R. M. Wald, *General Relativity*, (University of Chicago Press, Chicago, United States of America, 1983).
 - [10] S. W. Hawking, *Phys. Rev. Lett.* **26**, 1344 (1971).
 - [11] S. A. Hayward, *Phys. Rev. D* **49**, 831 (1994).
 - [12] S. A. Hayward, *Class. Quantum Grav.* **15**, 3147 (1998).
 - [13] S. G. Rubin, A. S. Sakharov and M. Yu. Khlopov, *J. Exp. Theor. Phys.* **92**, 921 (2001); M. Yu. Khlopov, S. G. Rubin and A. S. Sakharov, *Astropart. Phys.* **23**, 265 (2005).
 - [14] H. Kodama, M. Sasaki, K. Sato and K. Maeda, *Prog. Theor. Phys.* **66**, 2052 (1981).

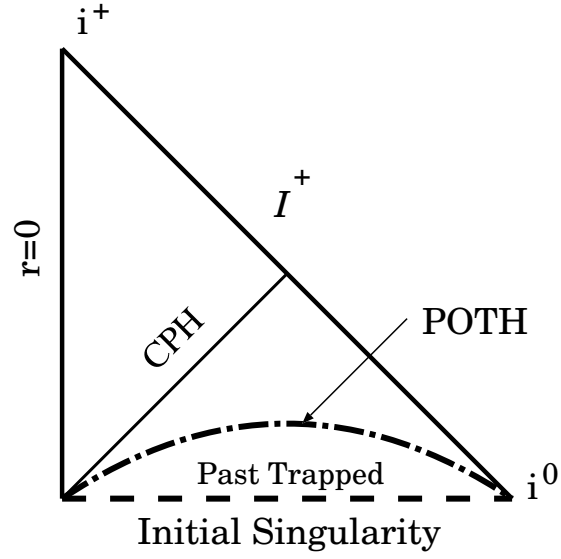


FIG. 1: The conformal diagram for a flat Friedmann spacetime with a massless scalar field. The cosmological apparent horizon, which is a past outer trapping horizon (POTH), is spacelike and outside the cosmological particle horizon (CPH).

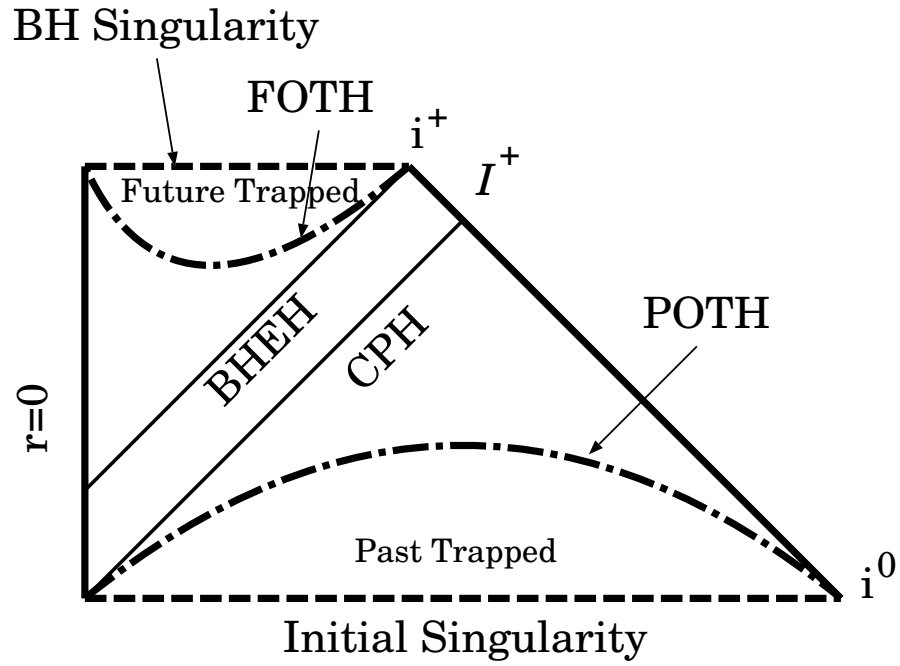


FIG. 2: The conformal diagram for a PBH smaller than the Friedmann cosmological particle horizon.

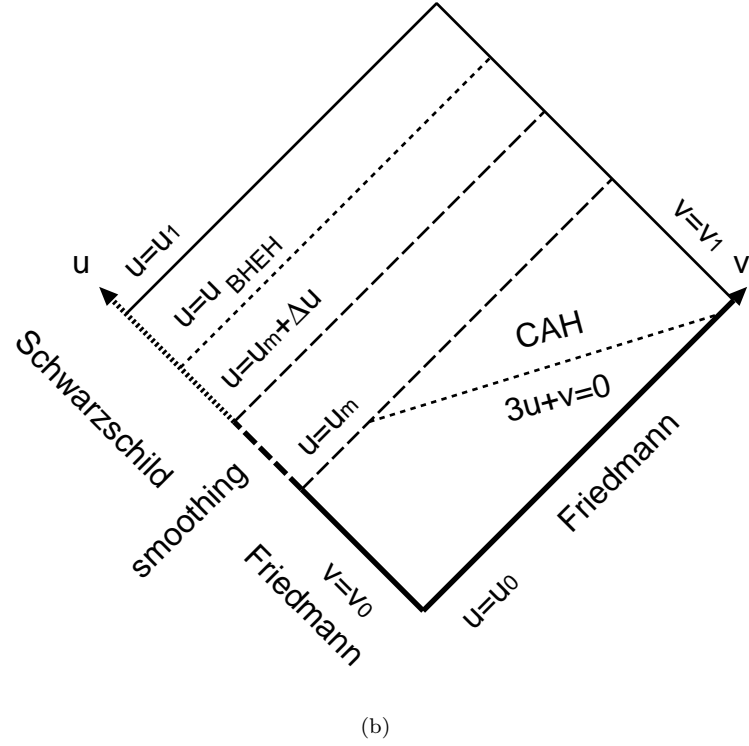
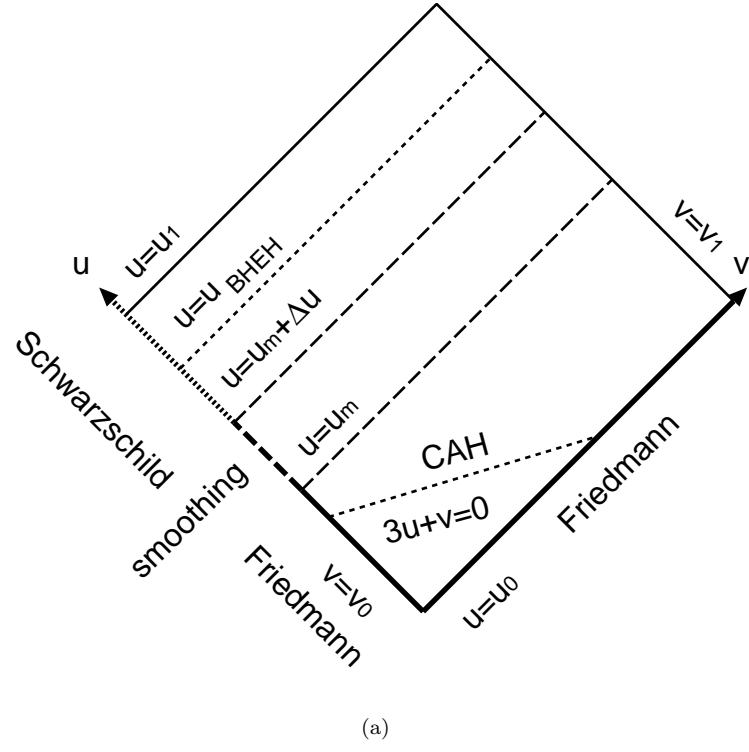
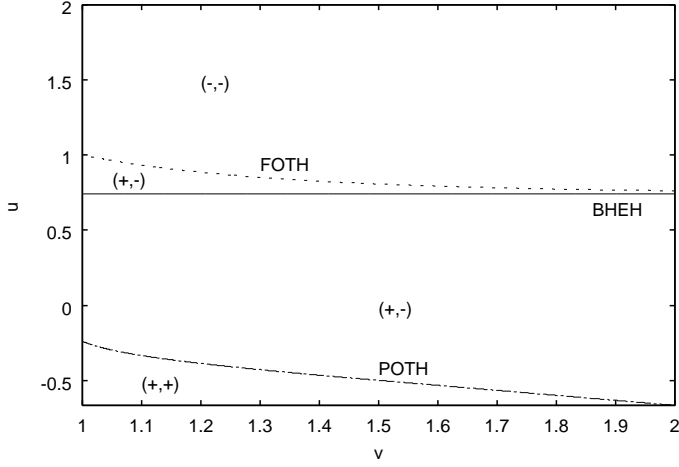
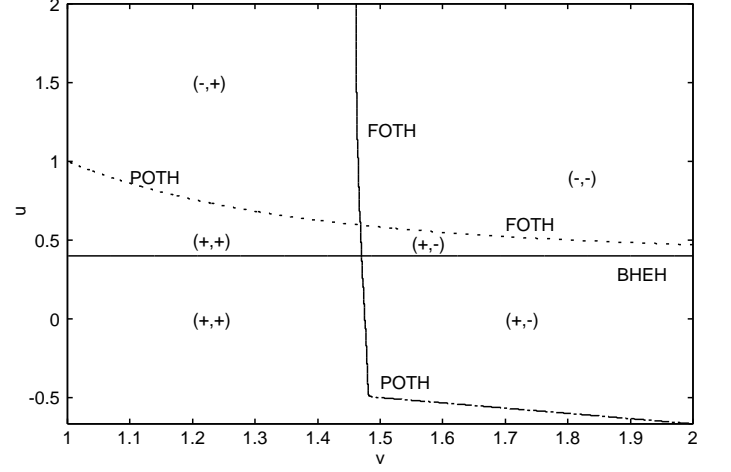


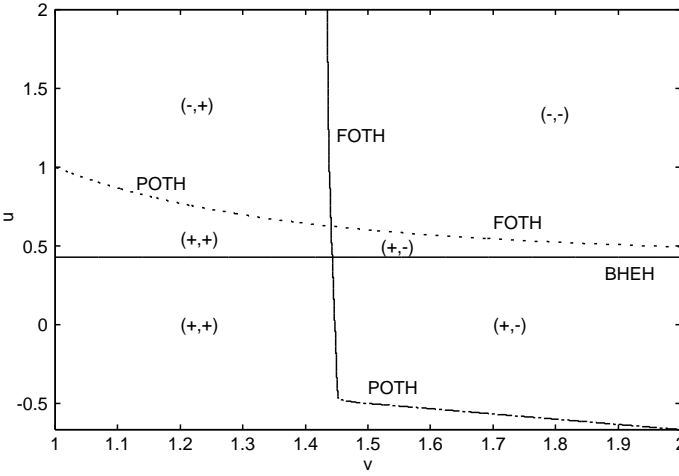
FIG. 3: Schematic figures for the initial data corresponding to PBHs (a) smaller and (b) larger than the cosmological apparent horizon (CAH).



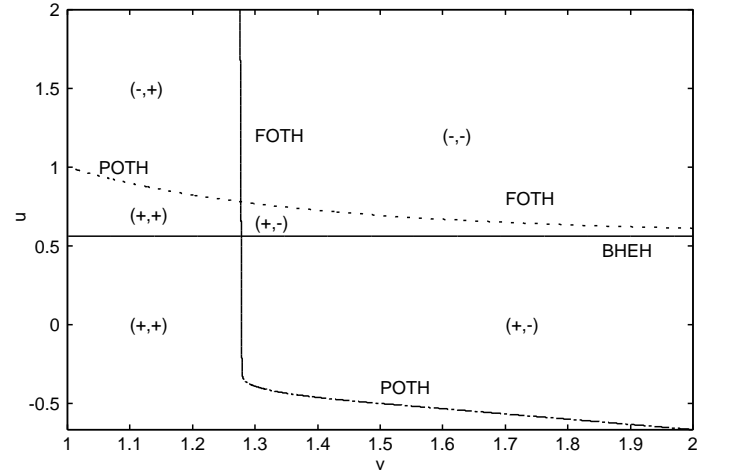
(a) E



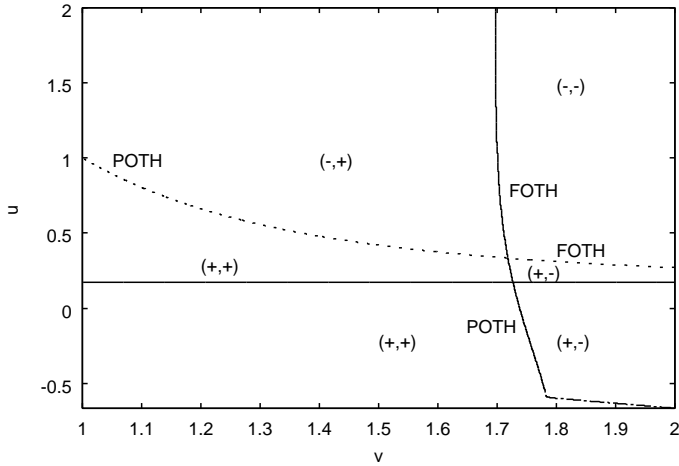
(b) F



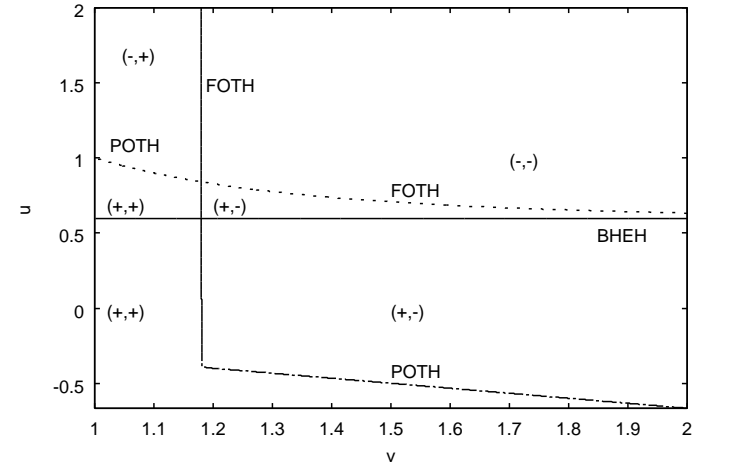
(c) G



(d) H

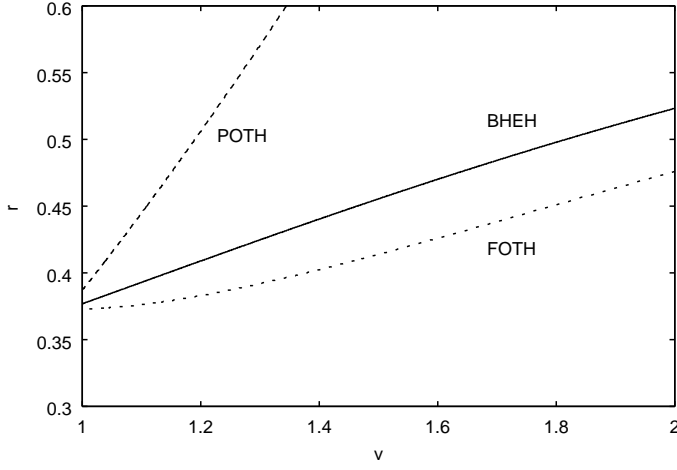


(e) I

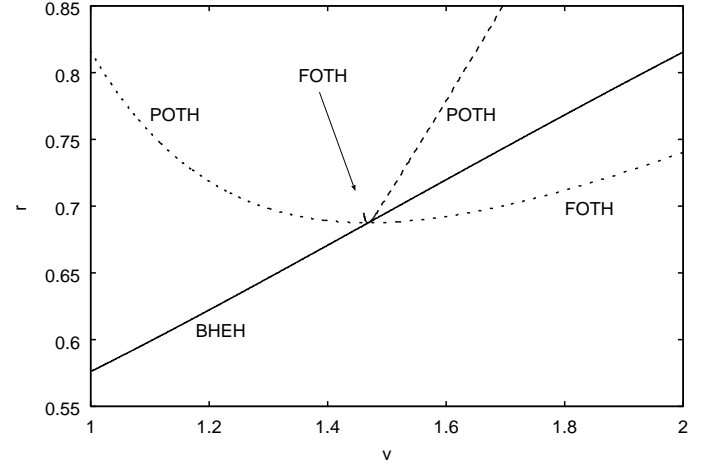


(f) J

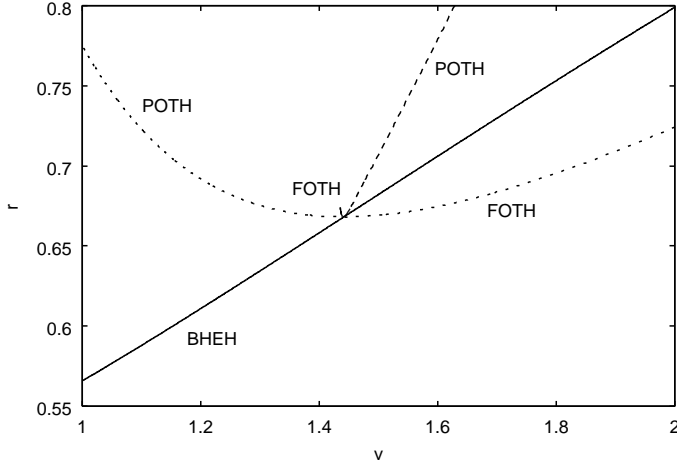
FIG. 4: Positions in (u, v) plane of black hole event horizon (BHEH) and trapping horizons with $r_{,v} = 0$ and $r_{,u} = 0$, plotted with solid, dashed and dotted-dashed lines, respectively. The future and past outer trapping horizons are labelled as “FOTH” and “POTH”, respectively. The signs of $(r_{,v})$ and $(r_{,u})$ are also shown. A region is future trapped if it has $(-, -)$, past trapped if it has $(+, +)$ and untrapped if it has $(+, -)$ or $(-, +)$.



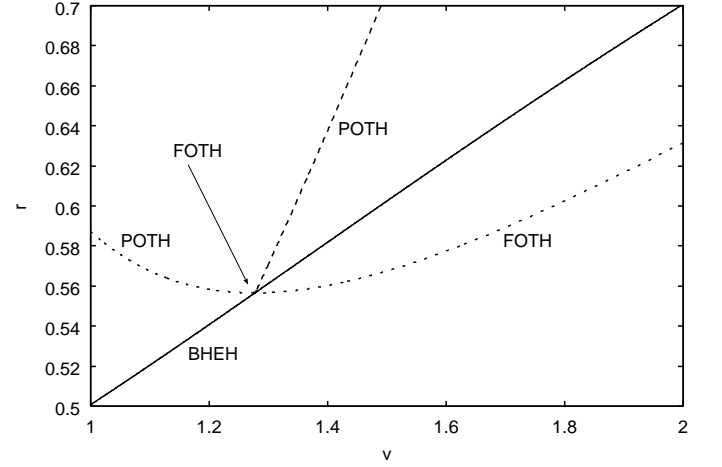
(a) E



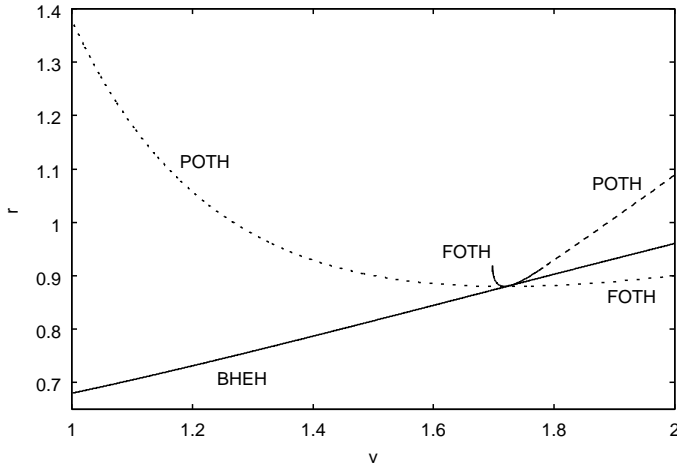
(b) F



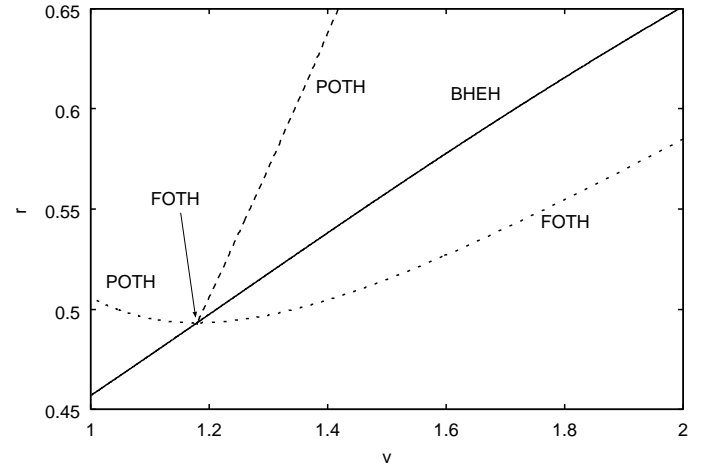
(c) G



(d) H

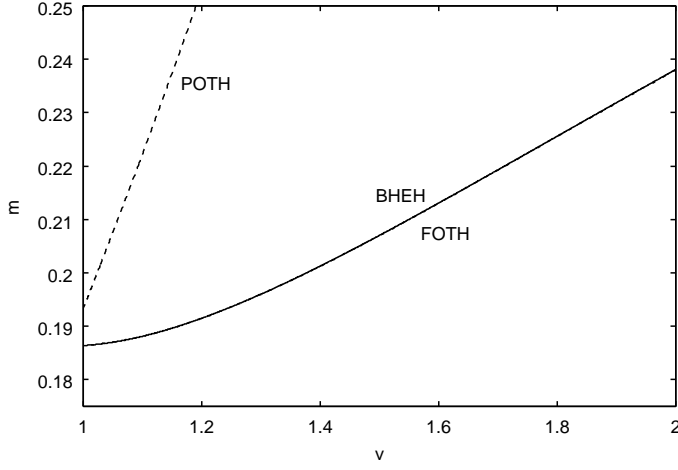


(e) I

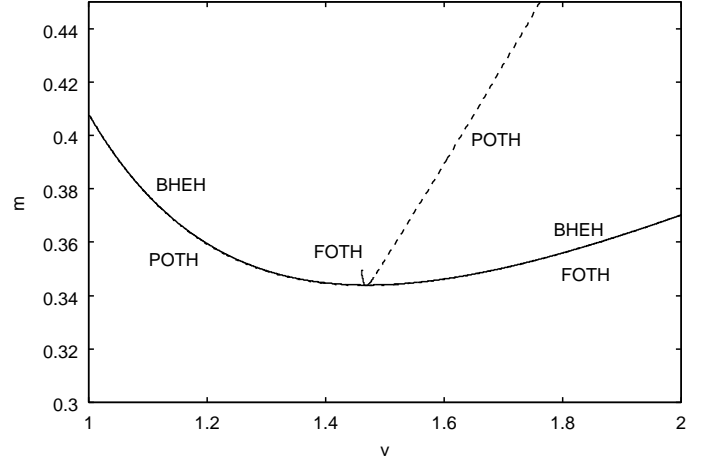


(f) J

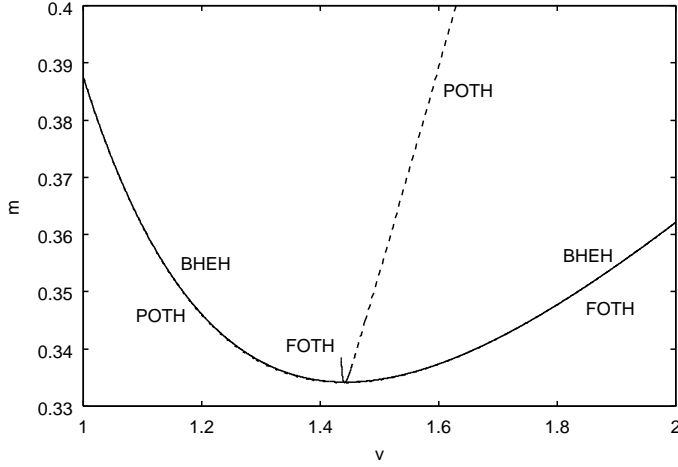
FIG. 5: The area radii of the black hole event horizon (BHEH) and trapping horizons with $r_{,v} = 0$ and $r_{,u} = 0$, plotted with solid, dotted and dashed lines, respectively. We can see the area radius of the black hole event horizon always increases.



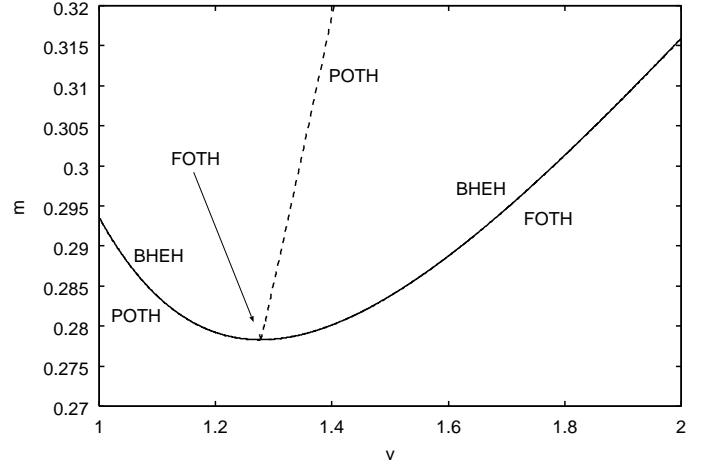
(a) E



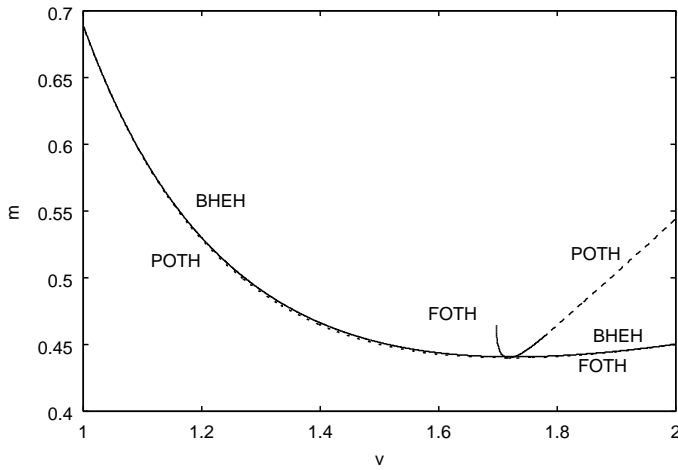
(b) F



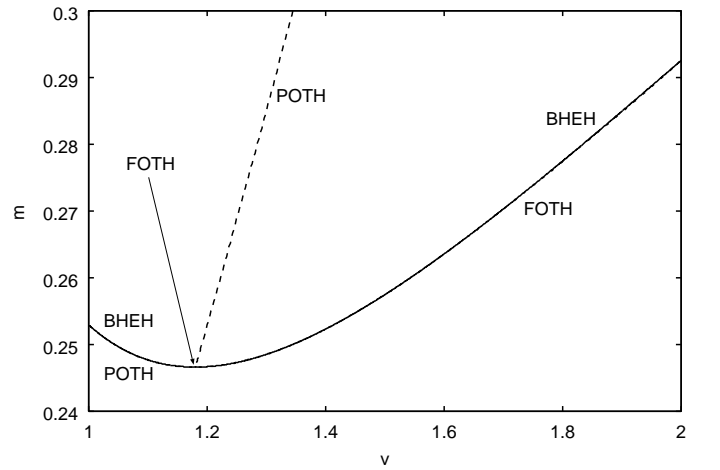
(c) G



(d) H



(e) I



(f) J

FIG. 6: The Misner-Sharp masses for the black hole event horizon (BHEH) and trapping horizons with $r_{,v} = 0$ and $r_{,u} = 0$, plotted with solid, dotted and dashed lines, respectively. The mass of the black hole event horizon decreases when it is in a past trapped region and increases when it is in a untrapped region with null expansions (+, -). The mass of the trapping horizon with $r_{,v} = 0$ is slightly larger than that of the black hole event horizon for each model, although they are almost indistinguishable.

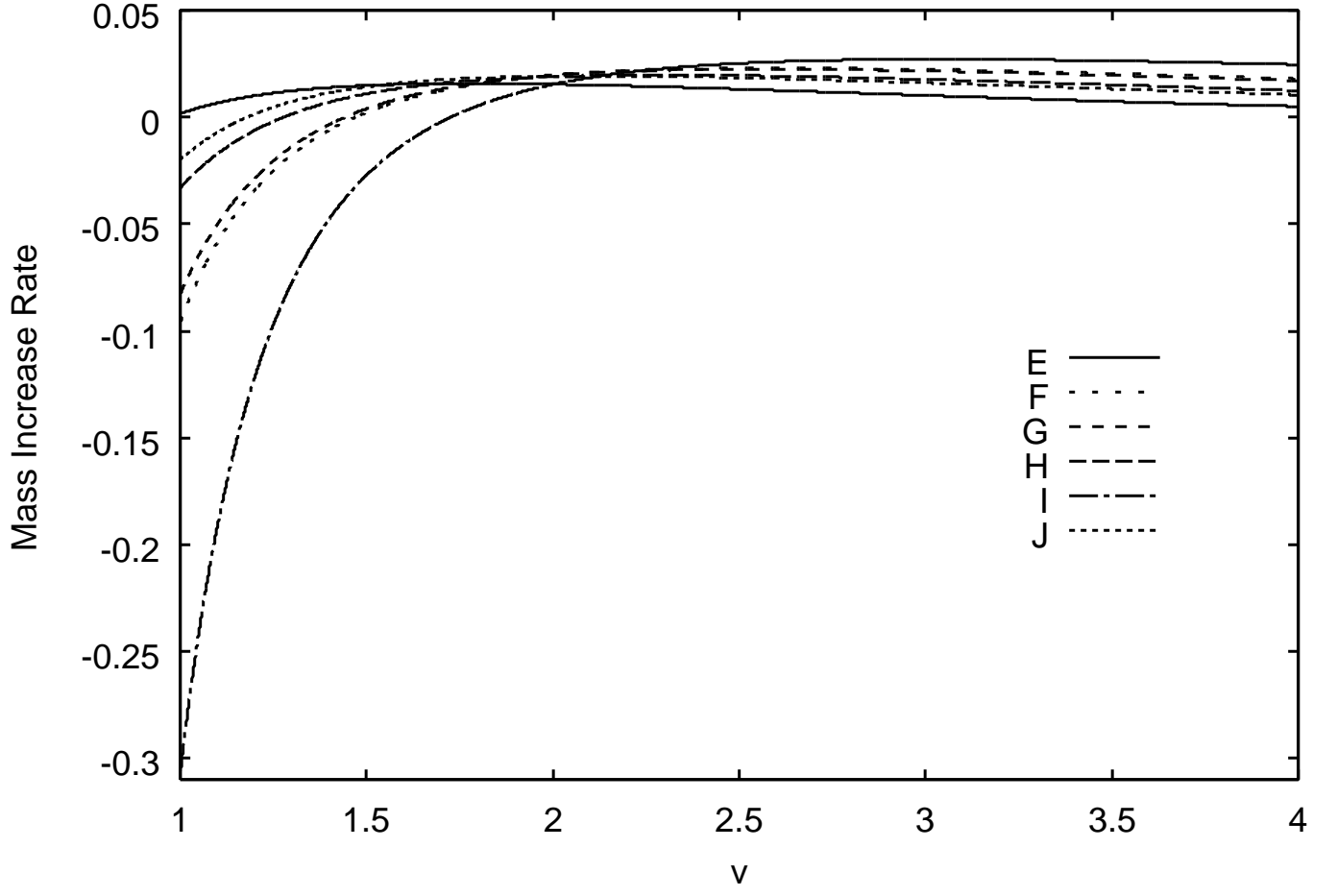


FIG. 7: Dependence of mass increase rate dm_{BHEH}/dv of the black hole event horizon on v for Models E–J. It is negative when the black hole event horizon is in the past trapped region but positive when it gets out of the past trapped region.

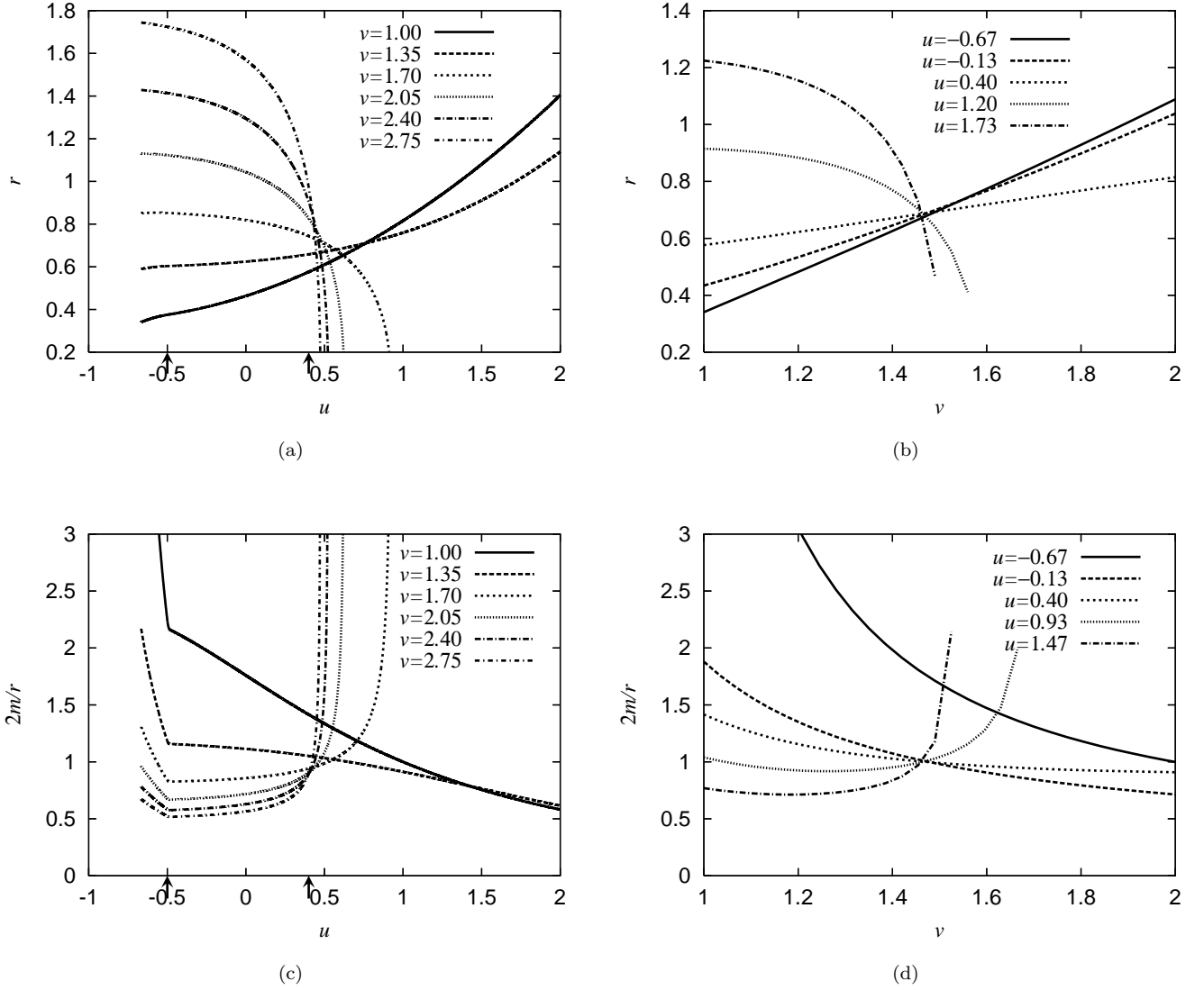


FIG. 8: The evolution of r along (a) $v = \text{const}$ and (b) $u = \text{const}$ and of $2m/r$ along (c) $v = \text{const}$ and (d) $u = \text{const}$ for Model F. In (a) and (c), the arrow at $u = -0.5$ denotes the matching surface, while the arrow at $u \simeq 0.400$ denotes the black hole event horizon.

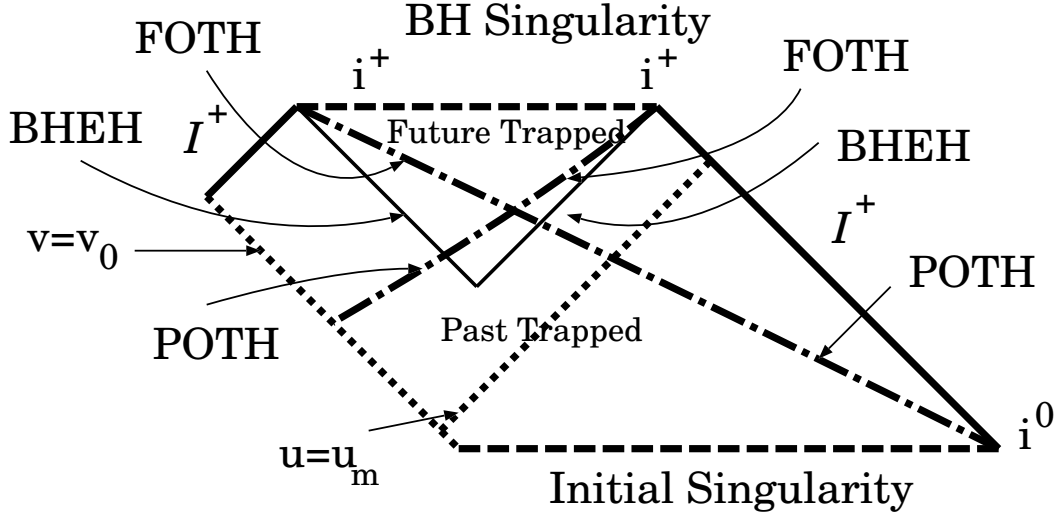


FIG. 9: Conformal diagram showing the possible causal structure for a PBH larger than the Friedmann cosmological apparent horizon. There are two distinct future null infinities and a past trapped (white hole) region is converted into a future trapped (black hole) region. The region with $u < u_m$ is the usual flat Friedmann spacetime but the region $v < v_0$ is not calculated. See text for details.

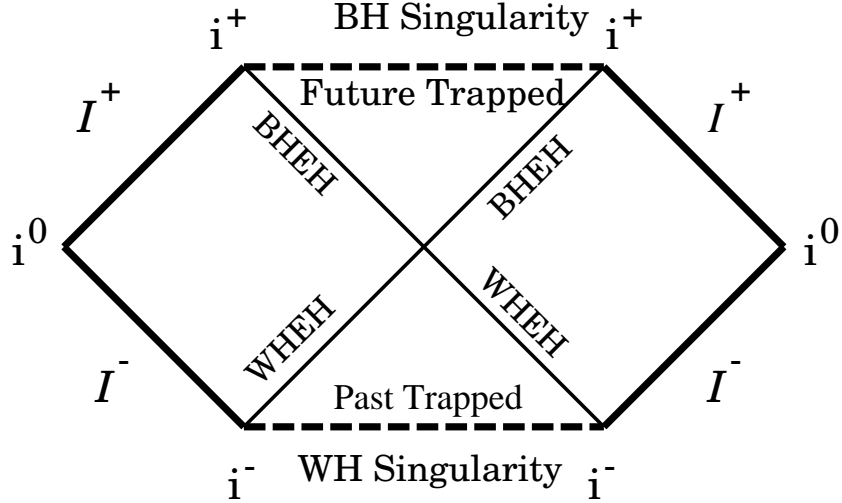


FIG. 10: Conformal diagram of the maximally extended Schwarzschild spacetime, i.e., the Kruskal diagram. The black hole event horizon (BHEH) coincides with the future outer trapping horizon and the white hole event horizon (WHEH) coincides with the past outer trapping horizon.

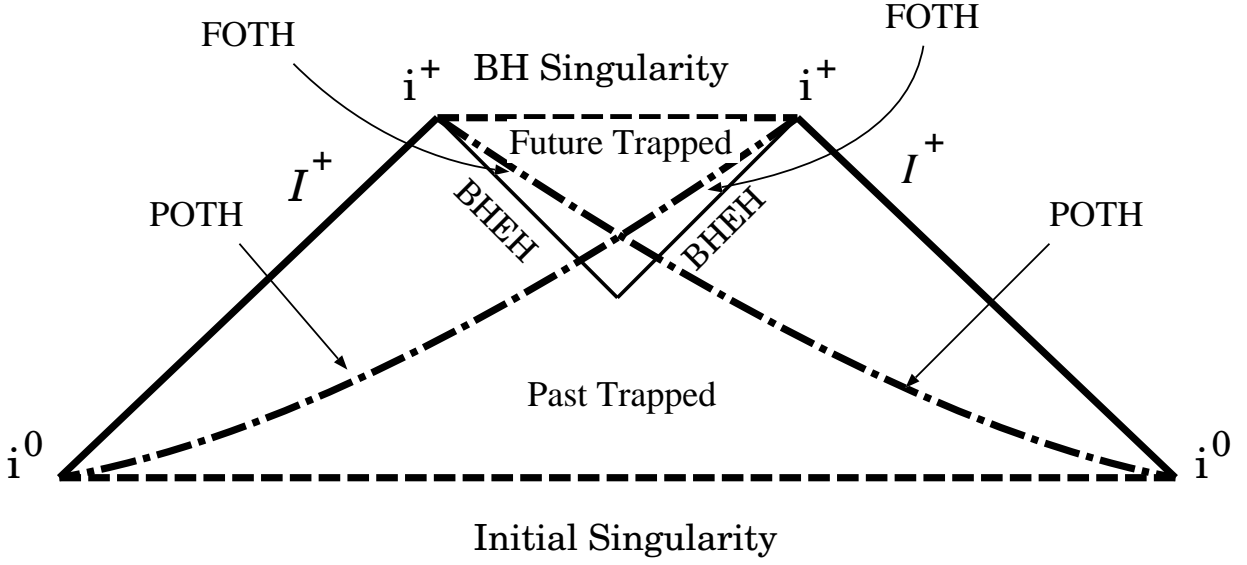


FIG. 11: Conformal diagram of a possible causal structure of the maximally extended spacetime for a PBH larger than the Friedmann cosmological apparent horizon. There are two distinct future null infinities, corresponding to the conversion of a past trapped (white hole) region into a future trapped (black hole) region.

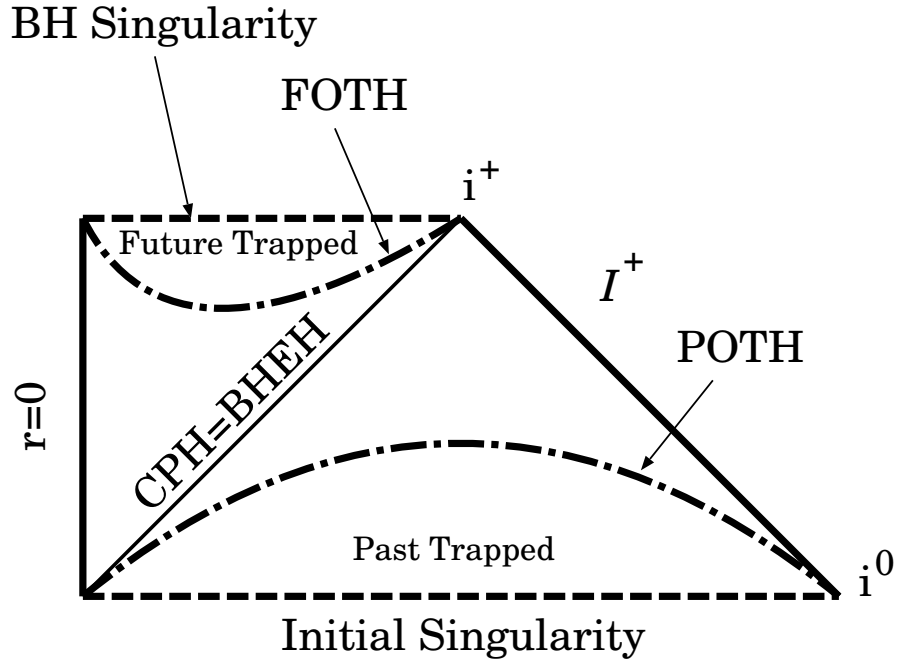


FIG. 12: Conformal diagram of the critical PBH spacetime, where the black hole event horizon (BHEH) coincides with the cosmological particle horizon (CPH).